



Adsorption and Photoelectrodeposition of Heavy Metal Ions from Wastewater using $\text{SnO}_{x(1 < X < 2)}$ / CeO_2 Photocatalysts

By Ryo Shoji, Yusaku Mochizuki, Yasukazu Kobayashi, Noriko Yamauchi
& Kazunori Sato

University of Tokyo

Abstract- Novel $\text{SnO}_{x(1 < x < 2)}$ / CeO_2 photocatalysts showed high adsorption and UV light-driven photoelectrodeposition activities for removal of heavy metal ions from water. The X-ray diffraction and the X-ray photoelectron spectroscopy analyses revealed that an amorphous $\text{SnO}_{x(1 < x < 2)}$ loaded on a high crystallinity CeO_2 . Amounts of Pb^{2+} removal of 20 wt% of SnO_x loading on CeO_2 were significantly higher than those of CeO_2 only and SnO_2 only due to the synergistic interaction between the high photocatalytic activity of the CeO_2 and the high adsorptive ability of the SnO_x . Results of Pb^{2+} removal indicated that the photoelectrodeposition occurred via adsorption of Pb^{2+} on the SnO_x surface with surface hydroxyl groups. Furthermore, it was suggested that not only Pb^{2+} but also Cu^{2+} , Cd^{2+} , Hg^{2+} , Se^{4+} , As^{3+} and Cr^{6+} can be removed by the $\text{SnO}_x/\text{CeO}_2$ photocatalysts. It is therefore expected that the $\text{SnO}_{x(1 < x < 2)}$ / CeO_2 can be used as the photocatalysts for purification of wastewater.

Keywords: *amorphous tin oxide, cerium oxide, Leads ion removal, photoelectrodeposition, wastewater treatment.*

GJRE-C Classification: FOR Code: 090499



Strictly as per the compliance and regulations of:



Adsorption and Photoelectrodeposition of Heavy Metal Ions from Wastewater using $\text{SnO}_{x(1 < X < 2)}/\text{CeO}_2$ Photocatalysts

Ryo Shoji ^α, Yusaku Mochizuki ^σ, Yasukazu Kobayashi ^ρ, Noriko Yamauchi ^ω & Kazunori Sato [¥]

Abstract- Novel $\text{SnO}_{x(1 < X < 2)}/\text{CeO}_2$ photocatalysts showed high adsorption and UV light-driven photoelectrodeposition activities for removal of heavy metal ions from water. The X-ray diffraction and the X-ray photoelectron spectroscopy analyses revealed that an amorphous $\text{SnO}_{x(1 < X < 2)}$ loaded on a high crystallinity CeO_2 . Amounts of Pb^{2+} removal of 20 wt% of SnO_x loading on CeO_2 were significantly higher than those of CeO_2 only and SnO_2 only due to the synergistic interaction between the high photocatalytic activity of the CeO_2 and the high adsorptive ability of the SnO_x . Results of Pb^{2+} removal indicated that the photoelectrodeposition occurred via adsorption of Pb^{2+} on the SnO_x surface with surface hydroxyl groups. Furthermore, it was suggested that not only Pb^{2+} but also Cu^{2+} , Cd^{2+} , Hg^{2+} , Se^{4+} , As^{3+} and Cr^{6+} can be removed by the $\text{SnO}_x/\text{CeO}_2$ photocatalysts. It is therefore expected that the $\text{SnO}_{x(1 < X < 2)}/\text{CeO}_2$ can be used as the photocatalysts for purification of wastewater.

Keywords: amorphous tin oxide, cerium oxide, lead ion removal, photoelectrodeposition, wastewater treatment.

I. INTRODUCTION

Heavy metal ions, such as lead, copper, cadmium, mercury, etc., existing in water are hazardous to the human health and the environmental ecosystem because of the high toxicity. These heavy metal ions are often found in industrial waste water from plating factories, paint manufactures, refinery plants, etc., and are difficult to be removed especially at low concentrations (Fu et al., 2011; Carolin et al., 2017). According to the drinking water standard of the World Health Organization (WHO) criteria, the concentration of heavy metal ions in discharged water is required to be decreased down to the ppb level, and it is too hard to meet this regulation standard at industrial processes of the developing countries (Chowdhury et al., 2016). The techniques which can remove various heavy metal ions at low concentrations with cost efficiency are therefore still necessary.

Author α: Department of Chemical Science and Engineering, National Institute of Technology, Tokyo College, Tokyo 193-0997, Japan.

Author ρ: Department of Chemical System Engineering, the University of Tokyo, Tokyo 113-8656, Japan.

Author ω: Department of Materials Science and Engineering, Ibaraki University, Ibaraki 316-8511, Japan.

Author ¥: Department of Materials Science and Technology, Nagaoka University of Technology, Niigata 940-2188, Japan.

Currently, there are several effective techniques for removal of heavy metal ions: chemical precipitation (Fu et al., 2011), ion exchange (Zewail et al., 2015), adsorption (Kumar et al., 2016), membrane filtration (Yurekli et al., 2017), electro dialysis (Nemati et al., 2017), reverse osmosis (Li et al., 2017), etc. Among them, the adsorption seems to be the most attractive technique due to its recovery merit, low cost, easy handling and simple design requirement (Kurniawan et al., 2006). However, it is difficult to remove the total metal ions by the only adsorption because of the physicochemical limitation of adsorptive rate particularly at the low concentration range of target metals. In contrast, a coupling method of the adsorption and the photoelectrodeposition is a more effective technique for the removing heavy metal ions at low concentrations due to utilizing irreversible photocatalytic redox reaction. Commonly, semiconductor photocatalysts have been used as an adsorbent to occur the photoelectrodeposition (Kobayashi et al., 2017; Nozaki et al., 2018).

The wide band gap semiconductors such as TiO_2 , WO_3 , SnO_2 , and CeO_2 have mostly been used as a photocatalyst due to their thermal and chemical stability, low cost and environmental-friendly (Ji et al., 2009; Zhang et al., 2018). Among them, the CeO_2 has received much attention for the unique characteristics. The CeO_2 possesses large oxygen storage and releasing ability derived from the redox cycle between Ce^{3+} and Ce^{4+} , and the CeO_2 is often utilized for the catalytic oxidation reaction. The CeO_2 therefore plays an important role as a photocatalyst for photo-oxidation and photo-reduction against adsorbed substances (Ke et al., 2014; Qiang et al., 2015). Furthermore, the CeO_2 shows a strong UV absorption and does not cause the photolysis during the photocatalysis (Magesh et al., 2009), while only CeO_2 nanoparticles show low adsorption capacity of heavy metal ions. In the pioneering reports, improvement on the adsorption capacity was attempted by loading heterogeneous semiconductor materials possessing the high adsorption capacity and the high carrier conductivity for the surface photoelectrodeposition such as Gd_2O_3 (Ayawanna et al., 2015), La_2O_3 (Ayawanna et al., 2017), ZnO (Nozaki et al., 2018), etc., on the CeO_2 as an auxiliary catalyst. However, these metal oxides easily

eluted instead of the adsorption of heavy metal ions as an ion-exchange manner because of their higher ionization tendency (Ayawanna et al., 2015; Ayawanna et al., 2017; Nozaki et al., 2018). Thus, an excellent loading material possessing high adsorption capacity, high carrier conductivity and chemical stability was desired.

Tin-oxide compounds (SnO_x) are focused in this study. The SnO_x has prominent superiorities such as high abundance, non-toxicity, low ionization tendency, high adsorption capacity of heavy metal ions, and fast carrier mobility between band structure and surface (Hamdi et al., 2017; Dey, 2018). Thus, the SnO_x offers many technological applications such as photocatalysts (Zhao et al., 2018), solid-state gas sensors, and adsorbents for the removal of heavy metal ions (Kumar et al., 2016; Dey, 2018). Motivated by these factors, the SnO_x was loaded on the CeO_2 surface to prepare a new photocatalyst for the adsorption and the photoelectrodeposition of heavy metal ions.

The primary purpose of this study was to synthesize the $\text{SnO}_x/\text{CeO}_2$ photocatalysts and evaluate its removal ability of heavy metal ions especially lead ion (Pb^{2+}). In addition, it was also a major purpose to obtain further knowledge of the photoelectrodeposition phenomenon which detailed mechanism has not been elucidated yet.

II. MATERIALS AND METHODS

a) Chemicals and reagents

$\text{Ce}(\text{NO}_3)_3 \cdot 6\text{H}_2\text{O}$, citric acid, ethylene glycol, $\text{SnCl}_2 \cdot 2\text{H}_2\text{O}$, $\text{Pb}(\text{NO}_3)_2$, $\text{Cu}(\text{NO}_3)_2 \cdot 3\text{H}_2\text{O}$, CdCl_2 , HgCl_2 , Na_2SeO_3 , $\text{K}_2\text{Cr}_2\text{O}_7$, arsenic standard solution (As^{3+} 1000 ppm), $(\text{NH}_4)_6\text{Mo}_7\text{O}_{24} \cdot 4\text{H}_2\text{O}$, and L(+)-ascorbic acid were all purchased from Wako Pure Chemical Industries Co., Ltd. 4-(2-pyridylazo)-resorcinol was purchased from Dojindo Molecular Technologies Co., Ltd. 2,3-diaminonaphthalene and 1,5-diphenylcarbazine were purchased from Tokyo Chemical Industry Co., Ltd. All other reagents were at least of reagent grade and used without further purification. Milli-Q water was used for the preparation of all aqueous solutions.

b) Synthesis of $\text{SnO}_x/\text{CeO}_2$

CeO_2 was prepared by the polymerized complex method. Firstly, 10.0 g of citric acid was dissolved in 11.8 g of ethylene glycol with heating at 50 °C for 30 min under stirring at 600 rpm by a hot magnetic stirrer. Then, 5.0 g of $\text{Ce}(\text{NO}_3)_3 \cdot 6\text{H}_2\text{O}$ were added to the solution and heated at 200 °C for 1 h under stirring at 600 rpm. Finally, the obtained precursor gel was calcined at 350 °C for 1 h and then at 1000 °C for 5 h with a heating rate of 10°C/min (Kakahana et al., 1992).

$\text{SnO}_x/\text{CeO}_2$ were prepared by the impregnation method. The prepared CeO_2 nanoparticles the above- were impregnated in an aqueous solution of $\text{SnCl}_2 \cdot$

$2\text{H}_2\text{O}$, and the solution was heated at 150 °C under stirring at 400 rpm. After the evaporation of water, the obtained sample was calcined at 650 °C for 3 h with a heating rate of 10 °C/min (Murayama et al., 2017).

c) Characterization

The crystal phase and structure of the obtained photocatalysts were analyzed by the powder X-ray diffraction (XRD, D8 ADVANCE, Bruker AXS) with $\text{CuK}\alpha$ radiation. The chemical states and composition of the photocatalyst surface were identified using the X-ray photoelectron spectroscopy (XPS, PHI X-tool, ULVAC-PHI) operated with $\text{AlK}\alpha$ radiation. The Chemical Shifts were calibrated by fixing the C 1s peak of the surface carbonaceous contaminants at 284.8 eV. The Brunauer-Emmett-Teller (BET) specific surface area of the photocatalysts were elucidated using a BET surface area analyzer (Flowsorb III, Shimadzu). The morphology and microstructure of the photocatalysts were elucidated using a field emission scanning electron microscopy (FE-SEM, Quanta 250 FEG, FEI). Determination of the point of zero charge (pH_{PZC}) of the photocatalyst surface was employed according to the Park and Regalbuto's procedure (Park et al., 1995).

d) Removal of Pb^{2+}

An aqueous solution including 20.0 mg/L Pb^{2+} was prepared. Then, 0.130 g or 0.200 g of the $\text{SnO}_x/\text{CeO}_2$ photocatalyst particles were added into a 20.0 mL of the prepared aqueous solution in a 30 mL beaker. The suspension was stirred at 500 rpm for 150 min by a magnetic stirrer and was also being irradiated with a UV-LED light (NCSU033B, 7.8 mW/cm², 360-370 nm, NICHIA). Another similar experimental set was carried out on the same suspension under stirring in dark condition. After the experiments, the reaction suspension was sampled and filtered, and the pH of the filtrate was measured using a pH meter (PH-201, SAGA). The residual concentrations of Pb^{2+} in the filtrate was measured by the colorimetry with 4-(2-pyridylazo)-resorcinol at 520 nm (Kocyla et al., 2015). The effect of different initial pH on Pb^{2+} removal was examined. The pH was adjusted using either 0.10 M HCl or 0.10 M NaOH solutions.

In the time-course removal experiments of Pb^{2+} , 1.000 g of the $\text{SnO}_x/\text{CeO}_2$ photocatalysts were added into a 100.0 mL of the aqueous solution including 20.0 mg/L Pb^{2+} in a 100 mL beaker due to sampling 5.0 mL of the reaction suspension at designated times (10, 30, 60, 105 and 150 min). The obtained data were fitted to the pseudo first-order model (Equation (1)) and pseudo second-order model (Equation (2))(Lagergren et al., 1898; Ho et al., 1999):

$$q_t = q_m(1 - \exp(-k_1t)) \quad (1)$$

$$q_t = \frac{q_m^2 k_2 t}{(1 + q_m k_2 t)} \quad (2)$$

Where q_t (mg/g) is the adsorption capacity at time t (min), q_m (mg/g) is the maximum adsorption capacity, k_1 (/min) and k_2 (g/mg/min) are the equilibrium rate constant of pseudo first-order adsorption and pseudo second-order adsorption, respectively.

e) Removal of other heavy metal ions

In the removal experiments of heavy metal ions other than Pb^{2+} , an aqueous solution including 20.0 mg/L Cu^{2+} , Cd^{2+} , Hg^{2+} , As^{3+} , Se^{4+} , and Cr^{6+} was prepared with adjusting pH to about 5~6 by using 0.10 M HCl or 0.10 M NaOH solutions. After each removal experiments, the residual concentrations of Cu^{2+} , Cd^{2+} , and Hg^{2+} in the filtrate were measured by the inductivity coupled plasma atomic emission spectroscopy (ICP-AES, PS7800, and HITACHI). The residual concentrations of As^{3+} (As^{5+}), Se^{4+} (Se^{6+}), and Cr^{6+} in the filtrate were measured by the redox treatment and colorimetry with ammonium molybdate and ascorbic acid at 840 nm (Lenoble et al., 2003), 2,3-diaminonaphthalene at 489 nm and 1,5-diphenylcarbazine at 540 nm (Pedro et al., 2004; Hesamedini et al., 2018), respectively.

III. RESULTS AND DISCUSSION

a) Characterization of the obtained photocatalysts

The XRD analysis was implemented to investigate the crystal phase and structure of the obtained photocatalysts. Fig. 1 shows the XRD patterns of CeO_2 and 20 wt% $\text{SnO}_x/\text{CeO}_2$. In the XRD pattern of CeO_2 only, the diffraction peaks were in good agreement with those of the cubic fluorite-structured CeO_2 crystal phase (ICDD PDF# 00-004-0593), and the sharpness of the peaks demonstrated the obtained CeO_2 particles possessing high crystallinity. In the XRD pattern of the 20 wt% $\text{SnO}_x/\text{CeO}_2$ composites, no specific peaks were observed except for those of the CeO_2 phase. It was indicated that the loaded SnO_x existing as amorphous and highly dispersed small nanoparticles on the CeO_2 surface.

The XPS analysis was implemented to investigate the surface chemical states and composition of the obtained photocatalysts. Fig. 2a presents the survey spectrum of the 20 wt% $\text{SnO}_x/\text{CeO}_2$. The appearance of peaks which are attributed to the Ce 3d, Sn 3d, and O 1s implied the existence of the Ce, Sn, and O elements on the surface of the obtained photocatalysts, and no specific peaks which are attributed to the other elements were observed except the C 1s peak. To investigate the detailed chemical state of the Ce, Sn, and O elements, the high-resolution XPS spectra of the Ce 3d, Sn 3d_{5/2}, and O 1s were measured (Fig. 2b-d). In the spectrum of the Ce 3d (Fig. 2b), the de-convoluted peaks labeled U and V are corresponding to Ce 3d_{3/2} states and Ce 3d_{5/2} states, respectively. According to the literature, U_0 , U_2 , V_0 , V_2 , and V_3 are all the characteristic peaks of Ce^{4+} , and U_1

and V_1 are attributed to the photoemission from Ce^{3+} (Lu et al., 2016). The measured peaks therefore demonstrated the primary existence of a CeO_2 phase with a small Ce_2O_3 phase on the surface of the 20 wt% $\text{SnO}_x/\text{CeO}_2$. In the spectrum of the Sn 3d_{5/2} (Fig. 2c), the de-convoluted Sn 3d_{5/2} spectra showed two adjacent peaks located at 486.2 and 486.7 eV, corresponding to the Sn^{2+} and Sn^{4+} , respectively (Babu et al., 2018). The coexistence of these two peaks indicated the presence of the $\text{SnO}_{x(1-x<2)}$ on the photocatalyst surface. According to this coexisting of the two states and the XRD pattern is shown in Fig. 1, it was suggested that the amorphous state $\text{SnO}_{x(1-x<2)}$ nanoparticles loading on the CeO_2 with the high dispersion states. In the spectrum of the O 1s (Fig. 2d), three de-convoluted peaks located at 529.3, 530.7, and 531.8 eV were observed. The first two peaks at 529.3 and 530.7 eV are probably associated with the lattice oxygen (O^{2-}) in the stronger Ce-O band and Sn-O band, respectively. However, since the peaks of the O 1s of Ce_2O_3 , CeO_2 , SnO, and SnO_2 are very close, assignment of these peaks was puzzling. The last peak at a higher binding energy of 531.8 eV was attributed to the oxygen in defective sites or surface hydroxyl groups (Nagasawa et al., 1999; Ke et al., 2014). the presence of this peak indicated that much oxygen defects were generated on the SnO_x surface with the amorphous nature and H_2O molecules then entered the oxygen defects or coordinated to the Sn^{4+} exposed on the surface. Finally, the hydroxyl groups were formed at the surface. According to the literature, the surface hydroxyl groups can be the functional groups for the adsorption of heavy metal ions on the surface of metal oxides (Wu et al., 2018).

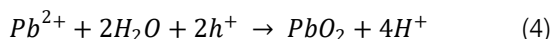
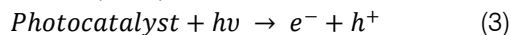
b) Removal of Pb^{2+}

To optimize amounts of the SnO_x loading on the CeO_2 , the relationship between amounts of the SnO_x loading and amounts of Pb^{2+} removal was examined as shown in Fig. 4. volumes of Pb^{2+} removal by the ADS and ADS + PED linearly increased along the increase of the amounts of the loaded SnO_x , up to 20 wt%. It was suggested that the SnO_x loaded on the CeO_2 was efficient for the improvement of a removal ability of Pb^{2+} because the available adsorption sites of Pb^{2+} are easily formed on the surface of the SnO_x . In the case of loading SnO_x more than 20 wt%, the amounts of the PED removal decreased than that of 20 wt% $\text{SnO}_x/\text{CeO}_2$. This result is because the existence ratio of the CeO_2 photocatalyst decreased along with the increase of the SnO_x ratio, and several photocatalytic active sites were physically covered by the excess SnO_x particles. Thus, the optimum amounts of the loaded SnO_x were 20 wt%.

Although the amorphous SnO_x has rich defect structures, it probably has the high mobility of the carrier due to the characteristics of the tin oxide compounds

(Dey, 2018). Also, according to the ICP-AES analysis, the ion-exchange elution of Sn ions and Ce ions were not detected in the removal process of Pb^{2+} . The promising usefulness of the SnO_x as a loading material was therefore reconfirmed.

Fig. 5 shows the time-course removal of Pb^{2+} by the 20 wt% $\text{SnO}_x/\text{CeO}_2$. Also, Table 1 shows the analyses of the Pb^{2+} adsorption kinetics of the 20 wt% $\text{SnO}_x/\text{CeO}_2$ by the pseudo first-order and the pseudo second-order models. As shown in Fig. 5, the adsorption did not reach equilibrium within 150 minutes, and for that, the pseudo second-order model was more suitable than the pseudo first-order model for describing the adsorption process. This result was probably explained by the adsorption of Pb^{2+} on the rough surface of the 20 wt% $\text{SnO}_x/\text{CeO}_2$ and the influence of the diffusion-limiting phenomenon. In previous reports, the adsorption of heavy metal ions to the metal oxides was said to be dominated by the process of ligand exchange with surface hydroxyl groups (-OH) on the metal oxides (Kumar et al., 2016), and tin oxide was considered to have more oxygen defects so that the hydroxyl groups are easily formed on the surface (Sun et al., 2018). The adsorption of Pb^{2+} to the 20 wt% $\text{SnO}_x/\text{CeO}_2$ is therefore very likely to occur through the surface hydroxyl groups. Focusing on the changes of Pb^{2+} removal by ADS + PED, it could be seen that the difference between the ADS and ADS + PED was definitely appeared after about 10 minutes. It was therefore suggested that the photoelectrodeposition occurred via the adsorption and induced further adsorption by oxidizing the adsorbed Pb^{2+} sequentially. Table 2 shows the pH changes of the reaction solution. In the ADS, the pH greatly decreased along with the progress of the adsorption of Pb^{2+} . This phenomenon seems to be because H^+ of the surface hydroxyl groups on the 20 wt% $\text{SnO}_x/\text{CeO}_2$ was replaced with Pb^{2+} . In the ADS + PED, the pH once decreased along with the progress of the Pb^{2+} adsorption. However, it could be seen that the pH increased along with the progress of the photoelectrodeposition of Pb^{2+} . After the experiments of the ADS + PED, the color of the $\text{SnO}_x/\text{CeO}_2$ suspension changed from light yellow to light brown. The adsorbed Pb^{2+} was probably oxidized as shown in the following equation previously reported by Kobayashi et al., (2017).



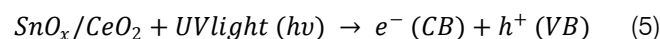
According to the above equation, the pH should decrease. It was hence considered that the increase of the pH was due to the elution of the surface hydroxyl groups (-OH) from the 20 wt% $\text{SnO}_x/\text{CeO}_2$ surface in the process of PbO_x deposition on the surface.

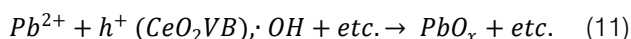
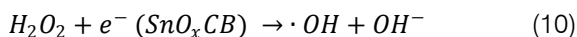
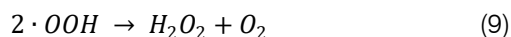
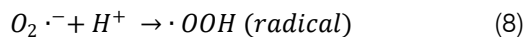
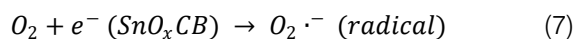
Fig. 6a shows the Pb^{2+} removal in the various initial pH and Fig. 6b shows the point of zero charge (pH_{PZC}) of the 20 wt% $\text{SnO}_x/\text{CeO}_2$. As shown in Fig. 6a, it

could be seen that the removal performance of Pb was drastically decreased at the pH below 3.5. The following three factors were assumed. (1) Since H^+ was released in the formation process of the surface hydroxyl groups, this process hardly proceeded under the acidic conditions. (2) In the adsorption process, Pb^{2+} displaced H^+ of the surface hydroxyl groups. Thus, it was unfavorable under the acidic conditions. (3) The estimated pH_{PZC} of the 20 wt% $\text{SnO}_x/\text{CeO}_2$ was 5.3 (Fig. 6b). Thus, under the acidic conditions, the surface hydroxyl groups were positively charged ($-\text{OH}_2^+$) and electrostatically repelled with Pb^{2+} (Ferreira et al., 2015). It was therefore considered that the 20 wt% $\text{SnO}_x/\text{CeO}_2$ photocatalysts are not suitable for use under the acidic conditions.

c) Mechanism of Pb^{2+} removal

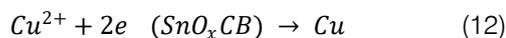
The mechanism of the adsorption and the photoelectrodeposition of Pb^{2+} by the 20 wt% $\text{SnO}_x/\text{CeO}_2$ photocatalysts is shown as the schematic diagram in Fig. 7. When the UV light is irradiated on the 20 wt% $\text{SnO}_x/\text{CeO}_2$, the electrons (e^-), which are ejected from valence band (VB) of the CeO_2 , move to the conduction band (CB) by creating the holes (h^+) in the VB (Equation (5)). While most of the electrons are recombined with the holes and disappeared, some electrons are quickly shifted to the SnO_x amorphous phase, and some holes are migrated to the CeO_2 surface (Priyadharsan et al., 2017). By the action of the generated carriers, Pb^{2+} adsorbed with the surface hydroxyl groups on the SnO_x is oxidized. The following three hypotheses are conceivable as a route to explain the oxidation reaction. (1) The holes on the CeO_2 surface act on nearby Pb^{2+} adsorbed on the SnO_x , and Pb^{2+} is oxidized (Kobayashi et al., 2017). (2) The holes on the CeO_2 surface generate hydroxyl radicals ($\cdot\text{OH}$) from OH^- (Equation (6)), and they oxidize Pb^{2+} on the SnO_x surface (Kumar et al., 2017). (3) The electrons on the SnO_x surface generate superoxide radicals ($\text{O}_2^{\cdot-}$) from dissolved oxygens (O_2) (Equation (7)). The superoxide radicals react with H^+ and produce peroxide radicals ($\cdot\text{OOH}$) (Equation (8)). These peroxide radicals finally interact with the electrons and form additional $\cdot\text{OH}$ radicals (Equations (9)-(10)) (Wang et al., 2017). As the adsorbed Pb^{2+} is then deposited as PbO_x on the photocatalyst surface (Equation (11)), some adsorption sites are regenerated, and the restriction of adsorption equilibrium is resolved. As a result, removal of Pb^{2+} further proceeds. The removal of Pb^{2+} is finally terminated by occupying all adsorption sites with the deposited PbO_x . The complete oxidation process can be understood by the following reaction steps (Kobayashi et al., 2017; Kumar et al., 2017; Priyadharsan et al., 2017; Wang et al., 2017):





d) Removal of other heavy metal ions

It was desired to extend the activity of the 20 wt% $\text{SnO}_x/\text{CeO}_2$ to the removal of other toxic heavy metal ions. The removal of Cu^{2+} , Cd^{2+} , Hg^{2+} , Se^{4+} , As^{3+} and Cr^{6+} as well as Pb^{2+} , were also investigated, and the results were shown in Fig. 8. The heavy metal ions other than Pb^{2+} could also be removed by the 20 wt% $\text{SnO}_x/\text{CeO}_2$ photocatalysts. The removal of Cu^{2+} was remarkably proceeded by the photoelectrodeposition. By the XPS analysis, it was revealed that the deposited material was the metallic Cu. The reduction of the Cu^{2+} adsorbed on the SnO_x were efficiently proceeded because of the smooth action of the excited electrons migrated to the SnO_x surface (Equation (12)) (Canterino et al., 2008).



SeO_3^{2-} and AsO_3^{3-} were efficiently adsorbed on the surface of the 20 wt% $\text{SnO}_x/\text{CeO}_2$, because oxygen atoms of the oxide anions easily entered to the oxygen defects or coordinated to the Sn^{4+} exposed on the surface of the amorphous SnO_x (Di et al., 2006). According to the XPS analyses, it was revealed that Se^{4+} and As^{3+} were deposited on the surface as SeO_2 and As_2O_3 after the ADS + PED. In contrast, $\text{Cr}_2\text{O}_7^{2-}$ could not be adsorbed at all on the surface of the 20 wt% $\text{SnO}_x/\text{CeO}_2$. It was therefore suggested that the 20 wt% $\text{SnO}_x/\text{CeO}_2$ cannot adsorb anything if adsorbate is an oxide anion. However, the reduction of Cr^{6+} by the excited electrons was slightly occurred (Ku et al., 2001). Thus, it can be suggested that the 20 wt% $\text{SnO}_x/\text{CeO}_2$ photocatalysts have a potential to remove various toxic heavy metal ions irrespective of cations or anions.

The 20 wt% $\text{SnO}_x/\text{CeO}_2$ could remove heavy metal ions at low concentrations by the adsorption and sequential photoelectrodeposition processes under the UV light irradiation. However, for practical applications, further improvement of adsorption capacity is desired (Fu et al., 2011). According to the previous reports, it was indicated that the adsorption performance can be enhanced by making the photocatalyst porous or loading the photocatalyst in a highly dispersed state on the substances having a high specific surface area such as zeolite, (graphene oxide, etc Setthaya et al., 2017; Li et al., 2018; Nozaki et al., 2018).

IV. CONCLUSION

The amorphous $\text{SnO}_{x(1<x<2)}$ loading on a high crystallinity CeO_2 photocatalysts were synthesized by

the polymerized complex method and the impregnation method for the adsorption and photoelectrodeposition of toxic heavy metal ions. The obtained photocatalysts were characterized by XRD, XPS, SEM, BET, and pH_{PZC} . According to the XRD and XPS analyses, the loaded SnO_x was composed of Sn^{2+} and Sn^{4+} and possessed numerous surface hydroxyl groups. In the removal of Pb^{2+} , a synergistic interaction between the photocatalytic activity of the CeO_2 and the adsorption ability of the SnO_x appeared efficiently when the amounts of SnO_x was 20 wt%. The photoelectrodeposition of Pb^{2+} occurred via adsorption of Pb^{2+} to the SnO_x with surface hydroxyl groups and progressed further removal. It was therefore indicated that the photoelectrodeposition showed a promoting effect of adsorption. In the acidic pH conditions, Pb^{2+} was almost not removed. Thus, it was suggested that the influence of surface hydroxyl groups of the 20 wt% $\text{SnO}_x/\text{CeO}_2$ was dominant for the adsorption of Pb^{2+} . A detailed Pb^{2+} removal mechanism was devised, suggesting the oxidation of Pb^{2+} by the action of holes and hydroxyl radicals. Furthermore, it was revealed that $\text{SnO}_x/\text{CeO}_2$ photocatalysts have a potential to remove various toxic heavy metal ions irrespective of cations or anions. It was therefore shown that $\text{SnO}_{x(1<x<2)}/\text{CeO}_2$ photocatalysts can purify various wastewater contaminated with heavy metal ions.

ACKNOWLEDGEMENTS

This work is supported by a joint research grant from Nagaoka University of Technology. Authors can describe any supports here.

Conflict of Interest

The authors have declared no conflict of interest.

REFERENCES RÉFÉRENCES REFERENCIAS

1. Ayawanna, J., Sato, K. (2017) 'Photoelectrodeposition Effect of Lanthanum oxide-Modified Ceria Particles on The Removal of Lead (II) Ions from Water', Catal. Today, in press.
2. Ayawanna, J., Teoh, W., Niratisairak, S., Sato, K. (2015) 'Gadolinia-modified ceria photocatalyst for removal of lead (II) ions from aqueous solutions', Mater. Sci. Semicond. Proc., vol. 40, pp. 136-139.
3. Babu, B., Reddy, I.N., Yoo, K., Kim, D., Shim, J. (2018) 'Bandgap tuning and XPS study of SnO_2 quantum dots', Mater. Letters, vol. 221, pp. 211-215.
4. Canterino, M., Somma, I.D., Marotta, R., Andreozzi, R. (2008) 'Kinetic investigation of Cu(II) ions photoreduction in presence of titanium dioxide and formic acid', Wat. Res., vol. 42, pp. 4498-4506.
5. Carolin, C.F., Kumar, P.S., Saravanan, A., Joshiba, G.J., Naushad, M. (2017) 'Efficient techniques for the removal of toxic heavy metals from aquatic

- environment: A review', *J. Environ. Chem. Eng.*, vol. 5, pp. 2782-2799.
6. Chowdhury, S., Mazumder, M.A.J., Attas, O.A., Husain, T. (2016) 'Heavy metals in drinking water: Occurrences, implications, and future needs in developing countries', *Sci. Total Environ.*, vol. 569-570, pp. 476-488.
 7. Dey, A. (2018) 'Semiconductor metal oxide gas sensors: A review', *Mater. Sci. Eng. B*, vol. 229, pp. 206-217.
 8. Di, Z.C., Ding, J., Peng, X.J., Li, Y.H., Luan, Z.K., Liang, J. (2006) 'Chromium adsorption by aligned carbon nanotubes supported ceria nanoparticles', *Chemosphere*, vol. 62, pp. 861-865.
 9. Ferreira, R.C., Couto Junior, O.M., Carvalho, K.Q., Arroyo, P.A., Barros, M.A.S.D. (2015) 'Effect of Solution pH on the Removal of Paracetamol by Activated Carbon of Dende Coconut Mesocarp', *Chem. Biochem. Eng. Q.*, vol. 29, pp. 47-53.
 10. Fu, F., Wang, Q. (2011) 'Removal of heavy metal ions from wastewaters: A review', *J. Environ. Manag.*, vol. 92, pp. 407-418.
 11. Hamdi, A.M.A., Rinner, U., Sillanpää, M. (2017) 'Tin dioxide as a photocatalyst for water treatment: A review', *Proc. Safety Environ. Protect.* vol. 107, pp. 190-205.
 12. Hesamedini, S., Bund, A. (2018) 'Formation of Cr (VI) in cobalt containing Cr (III)-based treatment solution', *Surf. Coat. Tech.*, vol. 334, pp. 444-449.
 13. Ho, Y., McKay, G. (1999) 'Pseudo-second order model for sorption processes', *Process Biochem.*, vol. 34, pp. 451-465.
 14. Ji, P., Zhang, J., Chen, F., Anpo, M. (2009) 'Study of adsorption and degradation of acid orange 7 on the surface of CeO_2 under visible light irradiation', *Appl. Catal. B*, vol. 85, pp. 148-154.
 15. Kakihana, M., Yoshimura, M. (1992) 'Polymerized complex synthesis and intergranular coupling of Bi-Pb-Sr-Ca-Cu-O superconductors characterized by complex magnetic susceptibility', *J. Appl. Phys.*, vol. 71, pp. 3904-3910.
 16. Ke, Y., Lai, S.Y. (2014) 'Comparison of the catalytic benzene oxidation activity of mesoporous ceria prepared via hard-template and soft-template', *Microporous Mesoporous Mater.*, vol. 198, pp. 256-262.
 17. Kobayashi, Y., Kanasaki, R., Nozaki, T., Shoji, R., Sato, K. (2017) 'Improving Effect of MnO_2 Addition on TiO_2 -Photocatalytic Removal of Lead Ion from Water', *J. Water Environ. Tech.*, vol. 15, pp. 35-42.
 18. Kocyla, A., Pomorski, A., Krężel, A. (2015) 'Molar absorption coefficients and stability constants of metal complexes of 4-(2-pyridylazo) resorcinol (PAR): Revisiting common chelating probe for the study of metallo proteins', *J. Inorg. Biochem.*, vol. 152, pp. 82-92.
 19. Kumar, K.Y., Raj, T.N.V., Archana, S., Prasad, S.B.B. Olivera, S., Muralidhara, H.B. (2016) ' SnO_2 nanoparticles as effective adsorbents for the removal of cadmium and lead from aqueous solution: Adsorption mechanism and kinetic studies', *J. Water Proc. Eng.*, vol. 13, pp. 44-52.
 20. Kumar, S., Kumar, A. (2017) 'Enhanced photocatalytic activity of rGO- CeO_2 nanocomposites driven by sunlight', *Mater. Sci. Eng. B*, vol. 223, pp. 98-108.
 21. Kurniawan, T.A., Chan, G.Y.S. Lo, W.H., Babel, S. (2006) 'Comparisons of low-cost adsorbents for treating wastewaters laden with heavy metals', *Sci. Total Environ.*, vol. 366, pp. 409-426.
 22. Ku, Y., Jung, I.L. (2001) 'Photocatalytic reduction of Cr (VI) in aqueous solutions by UV irradiation with the presence of titanium dioxide', *Wat. Res.*, vol. 35, pp. 135-142.
 23. Lagergren, S. (1898) 'Zurtheorie der sogenannten adsorption gelosterstoffe', *Kungliga Svenska Vetenskapsakademiens Handlingar*, vol. 24, pp. 1-39.
 24. Lenoble, V., Deluchat, V., Serpaud, B., Bollinger, J.C. (2003) 'Arsenite oxidation and arsenate determination by the molybdene blue method', *Talanta*, vol. 61, pp. 267-276.
 25. Li, X., Shen, R., Ma, S., Chen, X., Xie, J. (2018) 'Graphene-based heterojunction photocatalysts', *Appl. Surf. Sci.*, vol. 430, pp. 53-107.
 26. Li, Y., Xu, Z., Liu, S., Zhang, J., Yang, X. (2017) 'Molecular simulation of reverse osmosis for heavy metal ions using functionalized nanoporous-graphenes', *Comput. Mater. Sci.*, vol. 139, pp. 65-74.
 27. Lu, X., Li, X., Qian, J., Miao, N., Yao, C., Chen, Z. (2016) 'Synthesis and characterization of $\text{CeO}_2/\text{TiO}_2$ nanotube arrays and enhanced photocatalytic oxidative desulfurization performance', *J. Alloys Comp.*, vol. 661, pp. 363-371.3
 28. Magesh, G., Viswanathan, B., Viswannath, R.P., Varadarajan, T.K. (2009) 'Photocatalytic behavior of CeO_2 - TiO_2 system for the degradation of Methylene blue', *Indian J. Chem.*, vol. 48, pp. 480-488.
 29. Murayama, H., Hasegawa, T., Yamamoto, Y., Tone, M., Kimura, M., Ishida, T., Honma, T., Okumura, M., Isogai, M., Fujii, T., Tokunaga, M. (2017) 'Chloride-free and water-soluble Au complex for preparation of supported small nanoparticles by impregnation method', *J. Catal.*, vol. 353, pp. 74-80.
 30. Nagasawa, Y., Choso, T., Karasuda, T., Shimomura, S., Ouyang, F., Tabata, K., Yamaguchi, Y. (1999) 'Photoemission study of the interaction of a reduced thin film SnO_2 with oxygen', *Surf. Sci.*, vol. 433-435, pp. 226-229.
 31. Nemati, M., Hosseini, S.M., Shabaniyan, M. (2017) 'Novel electro dialysis cation exchange membrane

- prepared by 2-acrylamido-2-methylpropane sulfonic acid; heavy metal ions removal', *J. Hazard. Mater.* vol. 337, pp. 90-104.
32. Nozaki, T., Shoji, R., Kobayashi, Y., Sato, K. (2018) 'Feasibility of Macroporous CeO_2 photocatalysts for Removal of Lead Ions from Water', *Bullet. Chem. React. Eng. Catal.*, vol. 13, pp. 256-261.
 33. Park, J., Regalbuto, J.R. (1995) 'A Simple, Accurate Determination of Oxide PZC and the Strong Buffering Effect of Oxide Surfaces at Incipient Wetness', *Colloid Interface Sci.*, vol. 175, pp. 239-252.
 34. Pedro, J., Andrade, F., Magni, D., Tudino, M., onivardi, A. (2004) 'On-line sub micellaren hanced fluoro metric determination of Se(IV) with 2, 3-diaminonaphthalene', *Analyt. Chim. Acta*, vol. 516, pp. 229-236.
 35. Priyadharsan, A., Vasanthakumar, V., Karthikeyan, S., Raj, V., Shanavas, S., Anbarasan, P.M. (2017) 'Multi-functional properties of ternary $\text{CeO}_2/\text{SnO}_2/\text{rGO}$ nanocomposites: Visible light driven photocatalyst and heavy metal removal', *J. Photochem. Photobiol. A: Chem.*, vol. 346, pp. 32-45.
 36. Qiang, C., Wei, S., Lian, D., Binzhe, S., Xiaoxia, L., Aihua, X. (2015) 'A comparison between Ce(III) and Ce(IV) ions in photocatalytic degradation of organic pollutants', *J. Rare Earths*, vol. 33, pp. 249-254.
 37. Setthaya, N., Chindaprasirt, P., Yin, S., Pimraksa, K. (2017) ' TiO_2 -zeolite photocatalysts made of metakaolin and rice husk ash for removal of methylene blue dye', *Powder Tech.*, vol. 313, pp. 417-426.
 38. Sun, Y., Liu, T., Chang, Q., Ma, C. (2018) 'Study on the intrinsic defects in tin oxide with first-principles method', *J. Phys. Chem. Solids*, vol. 115, pp. 228-232.
 39. Wang, N., Pan, Y., Lu, T., Li, X., Wu, S., Wu, J. (2017) 'A new ribbon-ignition method for fabricating p-CuO/n-CeO₂ heterojunction with enhanced photocatalytic activity', *Appl. Surf. Sci.*, vol. 403, pp. 699-706.
 40. Wu, C., Tu, J., Tian, C., Geng, J., Lin, Z., Dang, Z. (2018) 'Defective magnesium ferrite nano-platelets for the adsorption of As(V): The role of surface hydroxyl groups', *Environ. Pollut.*, vol. 235, pp. 11-19.
 41. Yurekli, Y., Yildirim, M., Aydin, L., Savran, M. (2017) 'Filtration and removal performances of membrane adsorbers', *J. Hazard. Mater.*, vol. 332, pp. 33-41.
 42. Zewail, T.M., Yousef, N.S. (2015) 'Kinetic study of heavy metal ions removal by ion exchange in batch conical air spouted bed', *Alexandria Eng. J.*, vol. 54, pp. 83-90.
 43. Zhang, L., Jaroniec, M. (2018) 'Toward designing semiconductor-semiconductor heterojunctions for photocatalytic applications', *Appl. Surf. Sci.*, vol. 430, pp. 2-17.
 44. Zhao, D., Wu, X. (2018) 'Nanoparticles assembled SnO_2 nanosheet photocatalysts for wastewater purification', *Mater. Letters*, vol. 210, pp. 354-357.

Table 1: The analyses of the Pb^{2+} adsorption kinetics of 20 wt% $\text{SnO}_x/\text{CeO}_2$ by the pseudo first-order and pseudo second-order models

Pseudo first-order model		
k_1 (/min)	q_m (mg/g)	R^2
0.0152	0.620	0.941
Pseudo second-order model		
k_2 (g/mg/min)	q_m (mg/g)	R^2
0.00338	0.668	0.966

Table 2: Time-course changes of solution pH in the removal of Pb^{2+} using 20 wt% $\text{SnO}_x/\text{CeO}_2$ photocatalysts.

Time (min)	pH (Only ADS)	pH (ADS + PED)
0	5.5	5.5
10	4.3	4.4
30	4.2	4.4
60	4.2	4.5
105	4.1	4.7
150	4.1	4.9

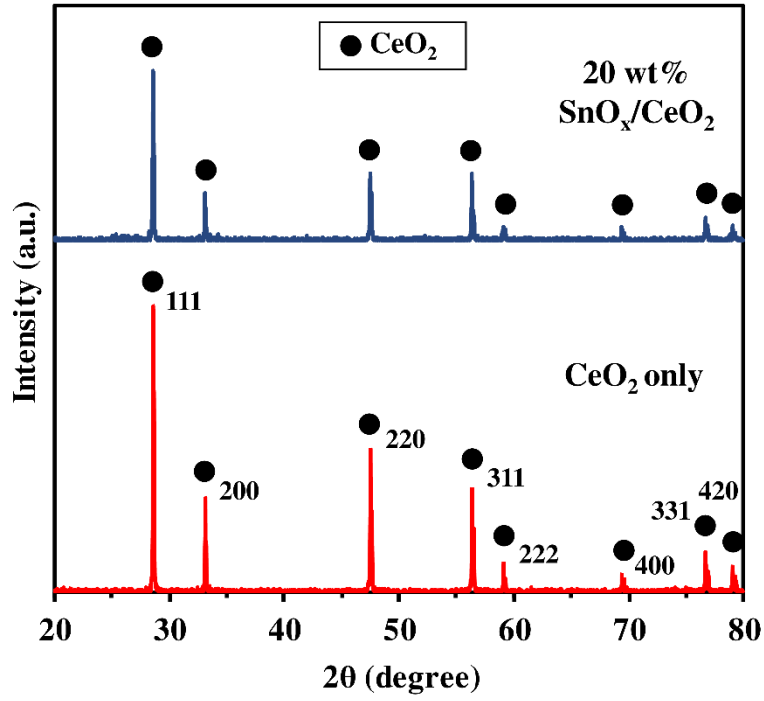
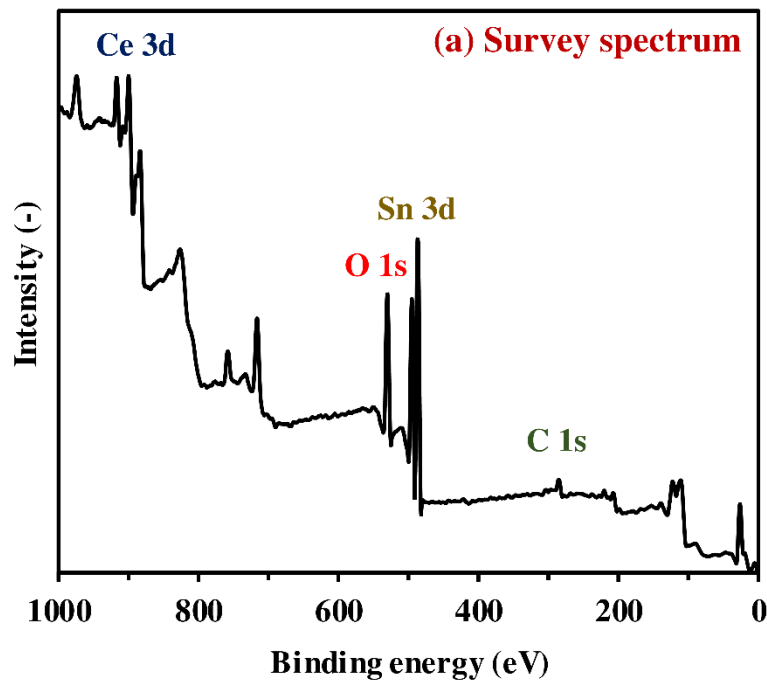
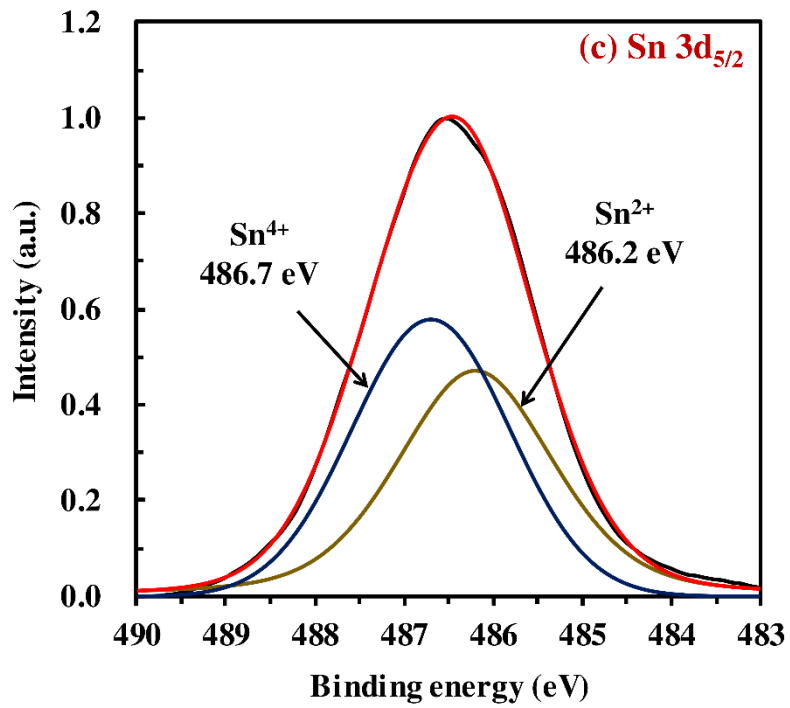
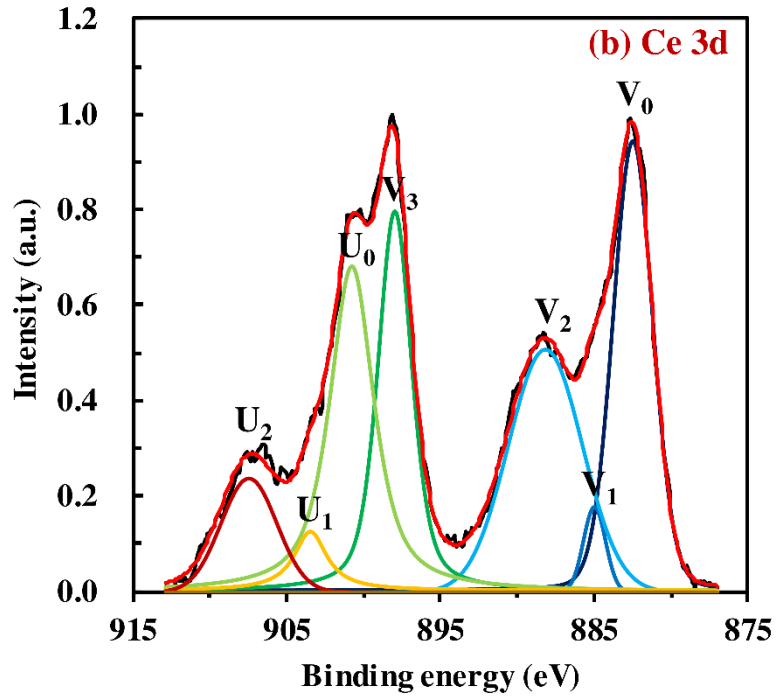


Figure 1: XRD patterns of CeO_2 only and 20 wt% $\text{SnO}_x/\text{CeO}_2$ photocatalysts





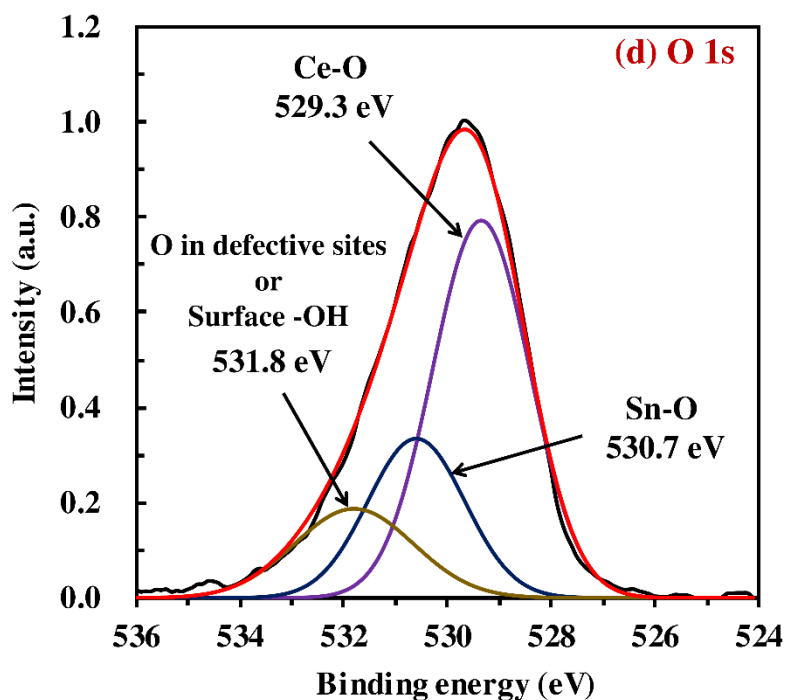


Figure 2: XPS spectra of 20 wt% $\text{SnO}_x/\text{CeO}_2$ photocatalysts: (a) survey spectrum, (b) Ce 3d, (c) Sn 3d_{5/2}, (d) O 1s.

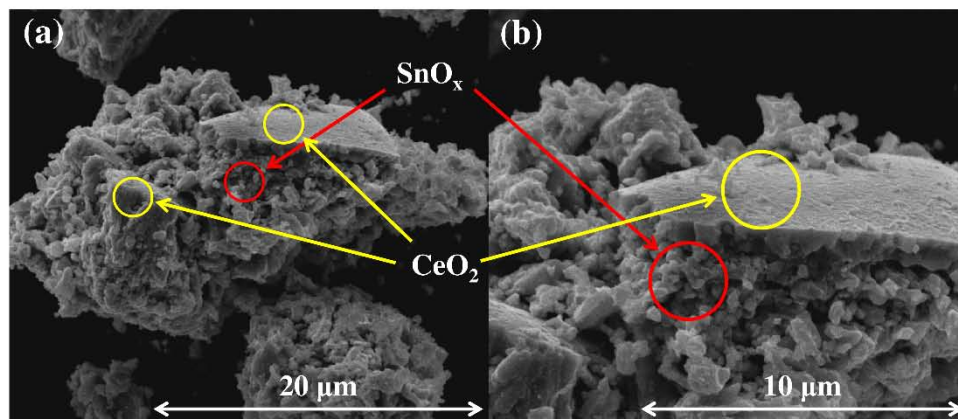


Figure 3: FE-SEM images of the synthesized 20 wt% $\text{SnO}_x/\text{CeO}_2$ composites at different resolutions (a b).

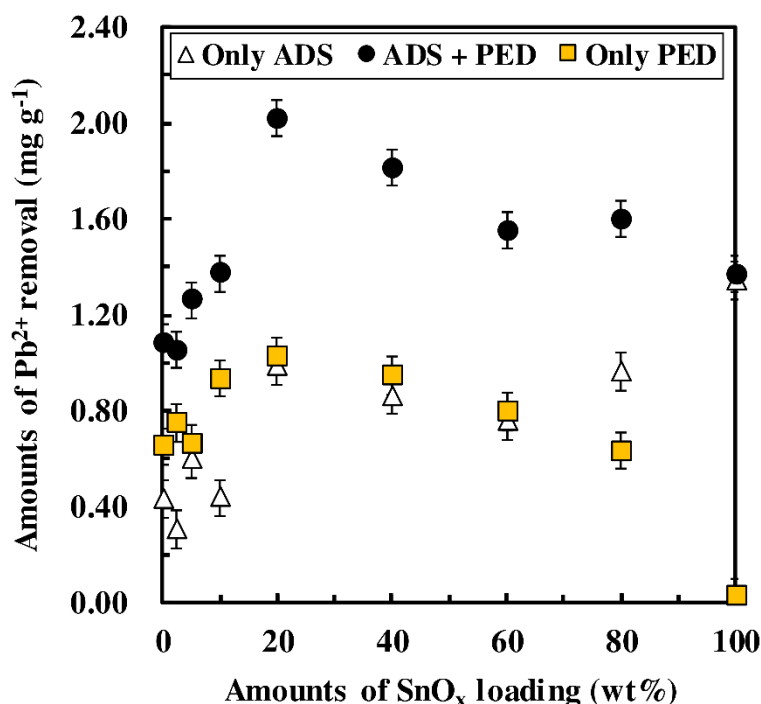


Figure 4: The relationship between amounts of the SnO_x loading and amounts of Pb^{2+} removal by only ADS, PED and ADS + PED, photocatalyst dosage: 0.130 g, solution volume: 20.0 mL, initial concentration of Pb^{2+} : 20.0 mg/L, initial pH: 5.5, test time: 150 min. ADS indicates the adsorption of heavy metal ions only by stirring under the dark condition, ADS + PED indicates the adsorption and photoelectrodeposition by stirring under UV light irradiation, and PED indicates the photoelectrodeposition meaning the difference of the Pb^{2+} removal amounts between the ADS and ADS + PED, respectively.

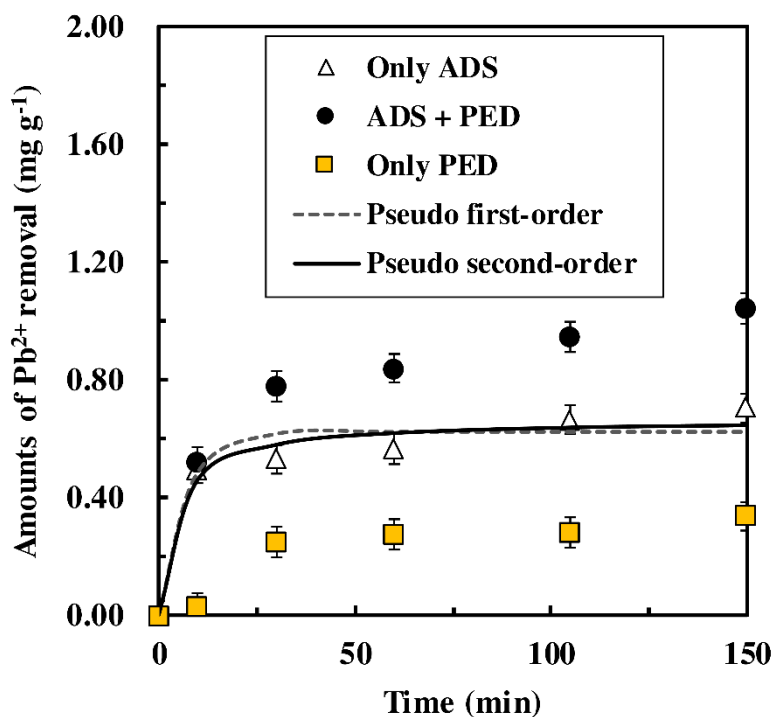


Figure 5: Time-course changes of amounts of Pb^{2+} removed by 20 wt% $\text{SnO}_x/\text{CeO}_2$ photocatalyst dosage: 1.000 g, solution volume: 100.0 mL, initial concentration of Pb^{2+} : 20.0 mg/L, initial pH: 5.5, test time: 150 min.

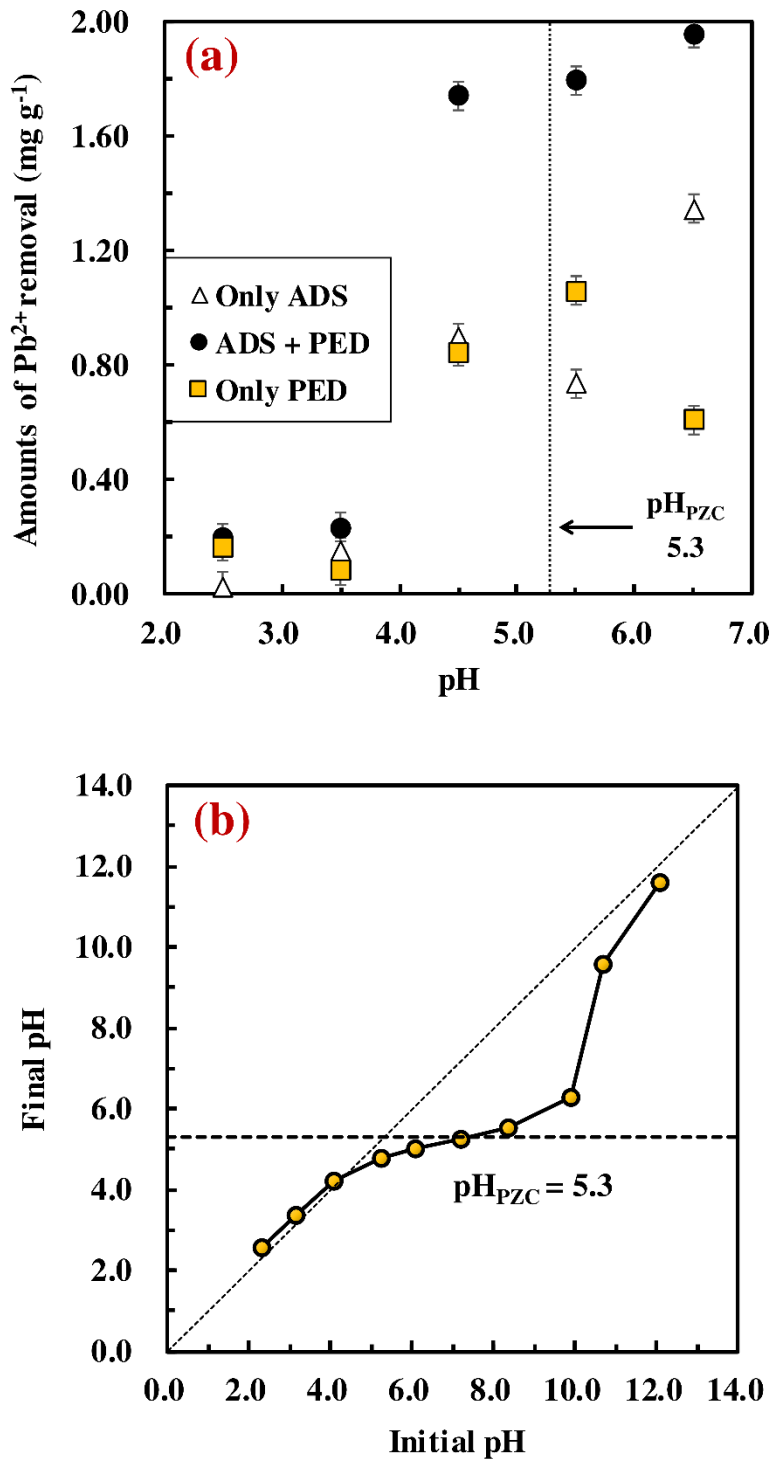


Figure 6: Effect of pH on the adsorption and photoelectrodeposition of Pb^{2+} by 20 wt% SnO_x/CeO photocatalysts, photocatalyst dosage: 0.200 g, solution volume: 20.0 mL, initial concentration of Pb^{2+} : 20.0 mg/L, initial pH: 2.5~6.5, test time: 150 min (a), and pH_{PZC} plots of the 20 wt% $\text{SnO}_x/\text{CeO}_2$ (b).

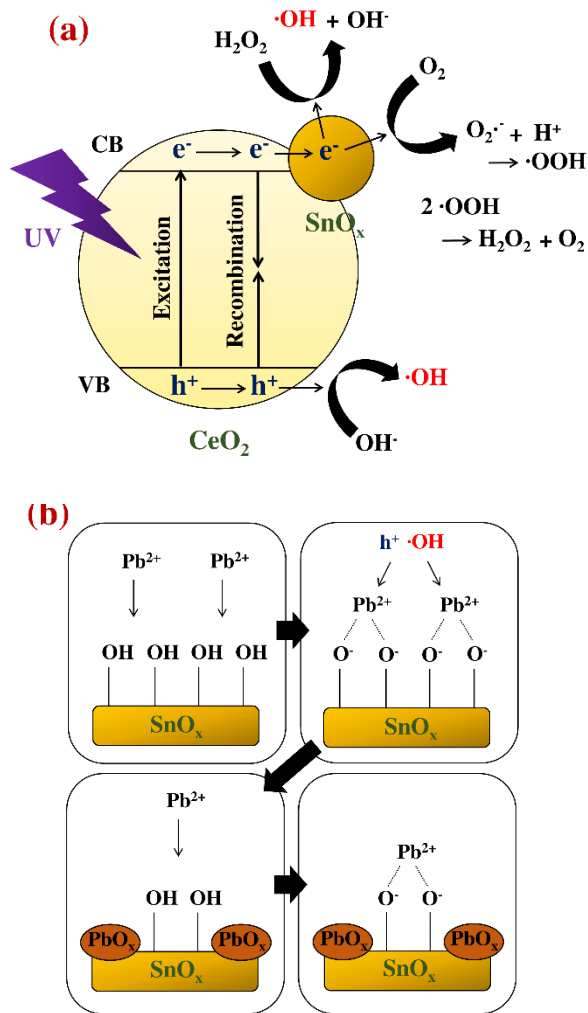


Figure 7: Schematic diagram for removal of Pb^{2+} by 20 wt% $\text{SnO}_x/\text{CeO}_2$ photocatalysts: (a) Generation of carriers for oxidation of Pb^{2+} , (b) Repetition of adsorption and photoelectrodeposition of Pb^{2+} .

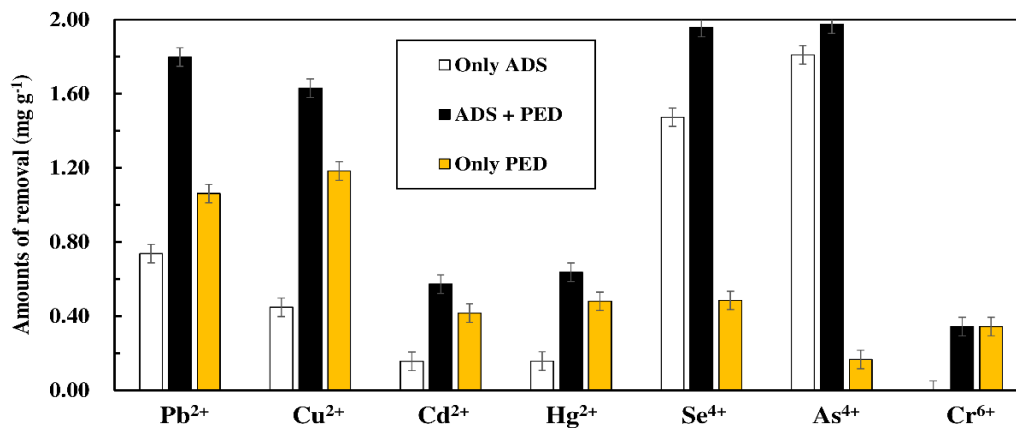


Figure 8: Amounts of Pb^{2+} , Cu^{2+} , Cd^{2+} , Hg^{2+} , Se^{4+} , As^{3+} , and Cr^{6+} removed by 20 wt% $\text{SnO}_x/\text{CeO}_2$ photocatalysts, photocatalyst dosage: 0.200 g, solution volume: 20.0 mL, initial concentration of each metal ions: 20.0 mg/L, initial pH: 5~6, test time: 150 min.